International Journal of Microwave and Wireless Technologies, 2010, 2(6), 523–530.
doi:10.1017/S1759078710000759

New extraction method of an equivalent circuit for an inductor in BiCMOS technology including lossy effects

LINH NGUYEN TRAN[1], EMMANUELLE BOURDEL[1], SEBASTIEN QUINTANEL[1] AND DANIEL PASQUET[2]

In order to perform an accurate design, in particular in non-linear circuit, the equivalent circuit of inductors must be precisely described in a wide frequency band. Many models have been proposed to describe the behavior of inductors on lossy substrate. They consist of a great number of elements, often suggested by physical phenomena. Most of them cannot be extracted from measurements. In this paper, we propose a model composed only of elements that can be analytically extracted from measurement results.

Keywords: Inductor, Silicon substrate, Lossy substrate, Eddy current, Magnetic coupling effects, Inductor model, Equivalent circuit, Integrated circuits, MMICs

Received 5 January 2010; Revised 23 August 2010

I. INTRODUCTION

Integrated spiral inductor is a key component in low noise amplifier, oscillators, filters, and impedance-matching networks. Therefore, inductor behavior studies in order to find out an equivalent electrical model should be considered. An accurate model will allow to anticipate and to improve the actual performance of the circuit.

Recently, a large number of works on integrated spiral inductors have been published [1–4]. However, lumped models were usually used for low frequencies (less than 10 GHz). Non-linear description of a circuit behavior needs a simulation up to the third-order harmonic. Starting with the introduction of new low-cost substrates such as silicon substrate, particular behaviors of inductor must be also considered and precisely described. The simplest model of an inductor on silicon substrate is given in Fig. 1 [1, 2], where L_s and R_s represent, respectively, series inductance and resistance of the integrated spiral inductor. The series feed forward capacitance C_s accounts for the capacitance due to the overlaps between the spiral and the center-tap underpass and between the spiral turns. The parasitic $C_{ox1,2}$ and $C_{sub1,2}$ capacitances represent, respectively, the coupling effects across oxide layers and silicon layer. Losses due to conductive substrate are modeled by $R_{sub1,2}$.

One of the drawbacks about the use of silicon technology in the microwave field is the substrate conductivity which is much greater than for III–V materials. This involves many physical phenomena at high frequencies like proximity effects, and particularly eddy current in the silicon substrate.

[1]ETIS Laboratory, CNRS, ENSEA University of Cergy Pontoise, UMR 8051, 6 avenue du Ponceau 95014 Cergy, France.
[2]LaMIPS, 2 rue de la Girafe, 14079 Caen, France. Phone: +33 6 33 73 64 99
Corresponding author:
D. Pasquet
Email: d.pasquet@ieee.org

However, the classical model (Fig. 1) is relatively simple and it does not contain elements that take into account the particular phenomena described above. Therefore, this model is only valid at lower frequencies and was then modified to many different types with different complexity to be more precise at higher frequencies. Generally, there are two major models: simple pi-model and double pi-model [3, 4]. Accuracy of these models compared to measurement is, therefore, significantly improved. Nevertheless, to achieve a greater accuracy, it is necessary to increase the model complexity [5–12]. Thus, elements in this kind of models are no more analytically extracted but are deduced by optimization procedure. Many elements are introduced by physical consideration but their value cannot be significantly reached from measurement [1, 5, 13].

In this paper, we propose a new pi-model deduced directly from measurements. Even if the usual inductance is used in a usual lower frequency band, we must not forget that non-linear simulations, using for instance harmonic balance, need an efficient description of the component up to the third or even fifth harmonic. Thus, all the elements in this model, which are frequency independent, are analytically extracted. The general approach consists of extracting a model directly from the measurement and interpreting each of its elements. This avoids having a large number of physically founded elements that remain impossible to reach from the measurements. The feasibility of this approach was verified by applying the obtained results on other inductors of different dimensions and different number of turns. We finally obtain an original equivalent scheme. The extraction method of the equivalent model and the comparison between the measurement results and those obtained from the extracted equivalent circuit is described in Section II. Section III describes an improved model of inductor whose elements are extracted by optimization procedure, simply to justify some previous results. In Section IV, we present the obtained results while applying the proposed equivalent

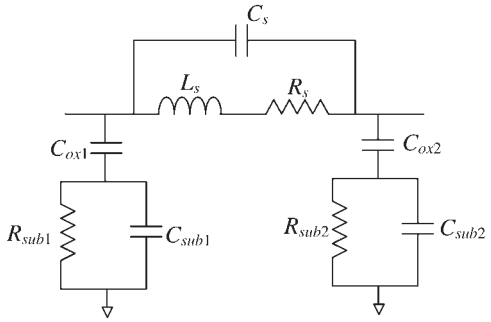

Fig. 1. Classical model of spiral inductor on silicon substrate [1, 2].

model and extraction procedures to two other inductors. Finally, Section V draws conclusions.

II. EXTRACTION OF THE MODEL PARAMETERS

We have measured a two-turn spiral inductor on a silicon substrate as shown in Fig. 2.

The outer diameter d is 200 μm, the strip width W, and the gap s between strips are, respectively, 20 and 3 μm which lead to a nominal inductance of 1 nH. The measurements have been carried out from 100 MHz to 40 GHz using a line-reflect-match calibration with an alumina calibration substrate [14]. The de-embedding process is based on a simplified representation of the accesses between the alumina substrate reference plane and the inductance reference planes as shown in Fig. 3. These accesses have been characterized by measuring a short in the inductor reference plane giving Z_1 and Z_3 then an open giving $Z_1 + Z_2$ and $Z_3 + Z_4$ [15]. The accesses lengths have been optimized in order to minimize Z_1 and Z_3.

A conversion from the measured S-parameters to Y-parameters simply leads to the pi topology in Fig. 4 [1, 13, 16, 17].

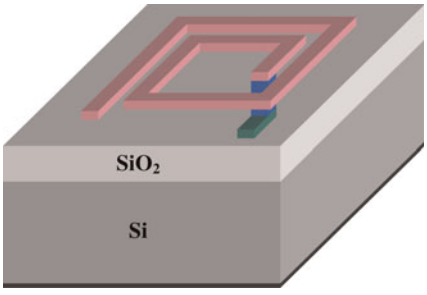

Fig. 2. Structure of the inductor on an SiGe substrate.

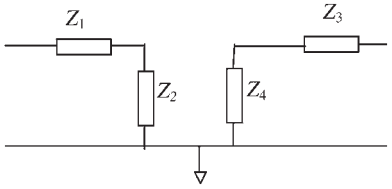

Fig. 3. Representation of the accesses.

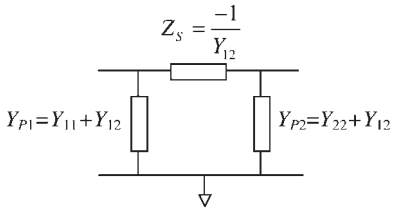

Fig. 4. Equivalent scheme of the inductor seen as a two-port represented by its admittance matrix.

A) Analytical extraction of the series part elements

The series impedance Z_S in Fig. 4 can be split into an inductive part L_S and a resistive part R_S in series, where

$$L_S = \frac{1}{\omega}\mathrm{Im}(Z_S), \tag{1}$$

$$R_S = \mathrm{Re}(Z_S). \tag{2}$$

The L_S and R_S variations against frequency are shown in Figs 5 and 6 where three frequency bands can be defined with regard to the inductor behavior. In region I, at low frequencies, the equivalent inductance L_S decreases from a quasi-static value to a constant value. In region II, it increases lightly. This equivalent inductance grows up quickly and then falls down in region III, like in a resonance. For the equivalent resistance R_S, in regions II and III, it becomes negative. This

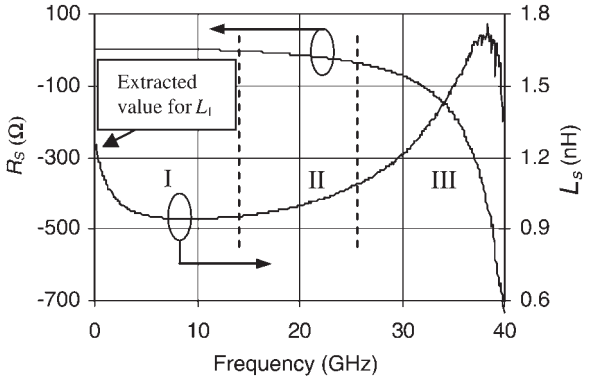

Fig. 5. Variation of the equivalent series part versus frequency.

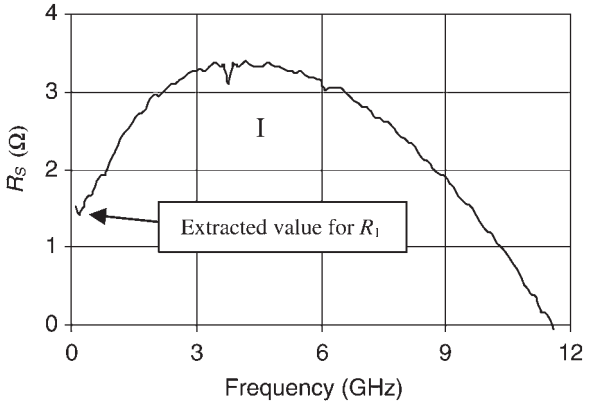

Fig. 6. Variation of the equivalent series resistance at low frequency.

https://doi.org/10.1017/S1759078710000759 Published online by Cambridge University Press

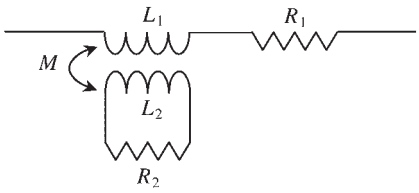

Fig. 7. Equivalent circuit of the series part of the inductor in regions I and II.

phenomenon suggests that a pi representation leads to non-physical results. We will go back to this in Section III.

In region I, the behavior of Z_S, especially for L_S, suggests a magnetic coupling shown in the electrical scheme in Fig. 7 [2, 5, 18–24]. The values of L_1 and R_1 appear, respectively, as quasi-static values of L_S and R_S. These values can be read directly on the ordinate axes of Figs 5 and 6.

This kind of transformer describes the eddy currents in the silicon substrate and in the surrounding metals, including spiral metal and ground metal. L_2, R_2, and M are not significant by themselves because they are not related to well-defined voltages and currents. They are perceived from the primary of the transformer by the coupling coefficient $k = (M^2 / L_1 L_2)$ and the relaxation time $\tau = (L_2 / R_2)$. Hence, in the frequency band of region I, impedance of the series part of inductor, Z_I could be approximated by

$$Z_S \approx Z_I = R_1 + jL_1\omega + \frac{kL_1\omega^2\tau}{1 + j\omega\tau} \tag{3}$$

From equation (3), we can extract two parameters, k_{ex} and τ_{ex} as shown in equations (4) and (5). Then, k and τ are extracted from the curves of k_{ex} and τ_{ex} in region I where they become constant as shown in Figs 8 and 9 [18]:

$$k_{ex} = 1 - \frac{L_S}{L_1}, \tag{4}$$

$$\tau_{ex} = \left[\omega\sqrt{\frac{kL_1}{L_1 - L_S} - 1}\right]^{-1}. \tag{5}$$

In region II, from about 12 GHz, R_S becomes negative whereas L_S increases lightly. This is represented by the branch of a capacitance C_1 in series with a negative resistance R_3 [5], which appears at higher frequencies only, i.e. as shown in Fig. 10. This negative value for R_s does not correspond to

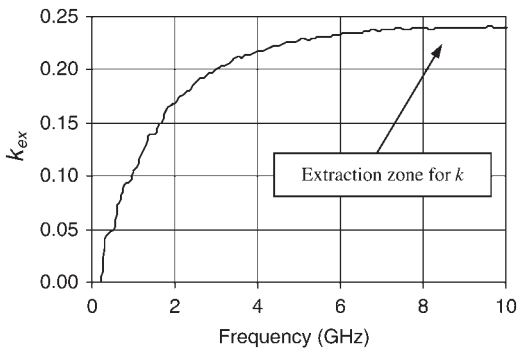

Fig. 8. Extraction of k.

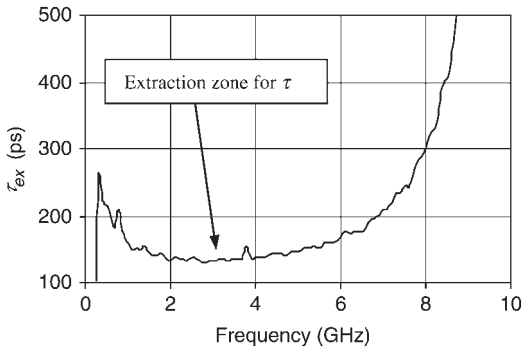

Fig. 9. Extraction of τ.

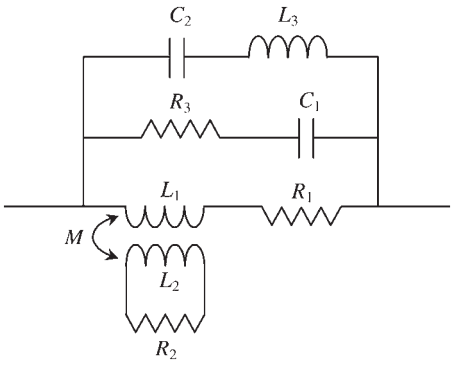

Fig. 10. Equivalent circuit of the series part of the inductor.

a physical phenomenon. This only proves that the physical behavior of the inductance is not completely described by a pi model. Actually, it is a combination of a pi and a tee models. We will return on this phenomenon at Section III.

At higher frequencies (region III), we have a resonance behavior of L_S. This behavior can be described by a series resonant L_3C_2 element in parallel as shown in Fig. 10.

Since the values for (C_1, R_3) and (C_2, L_3) are extracted independently, we perform the extraction of (C_1, R_3) at lower frequencies in region II, around 12 GHz to eliminate influence of C_2 and L_3. This extraction frequency must be also high enough to reduce the influence of the (L_1, R_1 L_2, R_2) elements used for low frequencies, which can affect the extraction result for C_1 and R_3. The extraction frequency has been then chosen at 15 GHz and the values for R_3 and C_1 are obtained from the two following expressions:

$$R_3 = \mathrm{Re}\left(\frac{Z_I Z_S}{Z_I - Z_S}\right), \tag{6}$$

$$C_1 = \left[\omega\mathrm{Im}\left(\frac{Z_S Z_I}{Z_S - Z_I}\right)\right]^{-1}. \tag{7}$$

Finally, the product L_3C_2 can be evaluated by the resonance frequency extrapolated from Fig. 5. The values for the elements of Fig. 10 are given in Table 1.

Figures 11 and 12 show the comparison up to 40 GHz for the series part of the inductor, represented by L_S and R_S, between the proposed model (Fig. 10) and the measurement results.

https://doi.org/10.1017/S1759078710000759 Published online by Cambridge University Press

Table 1. Extracted values for the equivalent circuit elements of the series part of the inductor.

L_1	R_1	k	τ	R_3	C_1	L_3	C_2
1.24 nH	1.4 Ω	0.246	133 ps	−800 Ω	24 fF	2.2 nH	4.6 fF

B) Analytical extraction of the parallel part elements

The parallel admittance (Y_{P_2}) in the right part of Fig. 3 can be split into an equivalent capacitance C_P and an equivalent resistance R_P in series, where

$$C_P = \frac{-1}{\omega}\left[\mathrm{Im}\left(\frac{1}{Y_{P_2}}\right)\right]^{-1}, \tag{8}$$

$$R_P = \mathrm{Re}\left(\frac{1}{Y_{P_2}}\right). \tag{9}$$

Figures 13 and 14 show their variations against frequency.

After a quasi-static behavior (at lowest frequencies), both capacitance and resistance decrease and tend to be constant at higher frequencies. Their evolution shapes versus frequency suggest the equivalent circuit in Fig. 15 [13–17, 19–27].

In Fig. 15 C_{R_1} corresponds to the part of electric field lines that pass through the SiO_2 layer and (C_{R_2}, R_{R_1}, R_{R_2}) correspond to the other part in the silicon substrate. The parallel

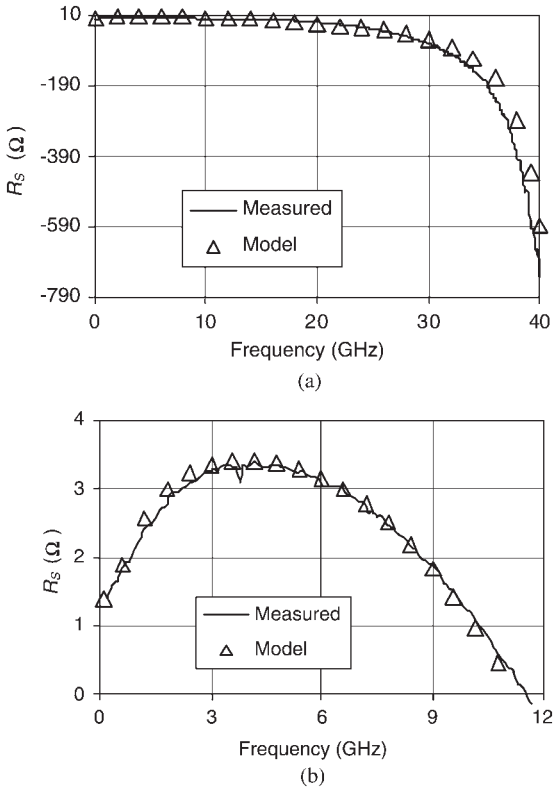

Fig. 11. Comparison of the equivalent resistance for the series part of the inductor between measurement and equivalent circuit: (a) for the whole frequency band and (b) at low frequency.

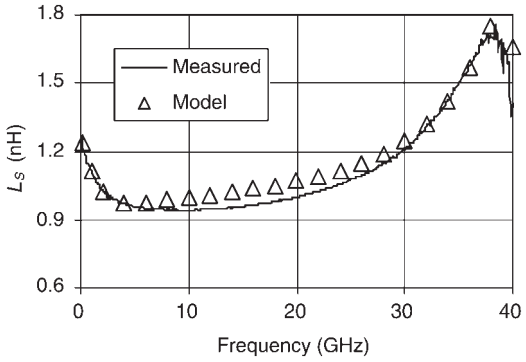

Fig. 12. Comparison of the equivalent inductance for the series part of the inductor between measurement and equivalent circuit.

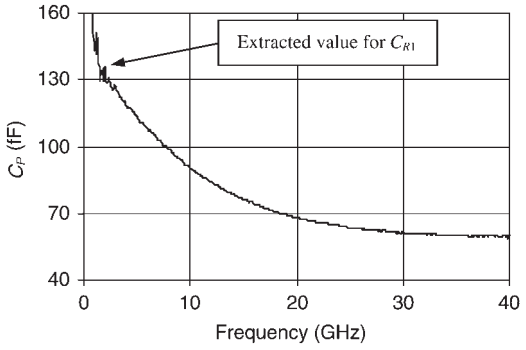

Fig. 13. Variation of the equivalent capacitance of the right parallel part of the inductor versus frequency.

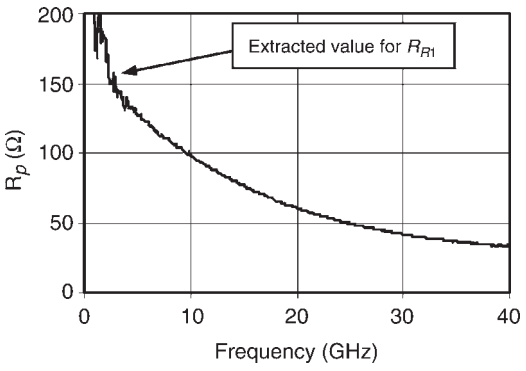

Fig. 14. Variation of the equivalent resistance of the right parallel part of the inductor versus frequency.

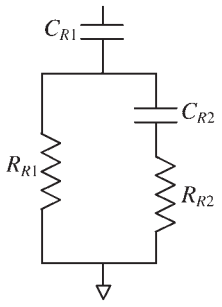

Fig. 15. Equivalent circuit of the parallel part of the inductor.

https://doi.org/10.1017/S1759078710000759 Published online by Cambridge University Press

terms become

$$R_P + \frac{1}{j\omega C_P} = \frac{1}{j\omega C_{R_1}} + \frac{R_{R_1}(1 + j\omega R_{R_2} C_{R_2})}{1 + j\omega C_{R_2}(R_{R_1} + R_{R_2})}, \qquad (10)$$

where C_{R_1} and R_{R_1} denote, respectively, the value of the C_P and R_P at low frequencies, which correspond to the quasi-static values on the ordinate axis. However, due to the calibration uncertainty at low frequencies, these quasi-static values are not precisely determined. We have taken the values for C_{R_1} and R_{R_1} at relatively low frequencies as shown in Figs 13 and 14. The tolerance of this extraction is not very important because the next extractions based on these values permit to approach the model from the measurement results for the whole frequency band.

The development of equation (10) gives the following expressions of C_{R2ex} and R_{R2ex}:

$$C_{R2ex} = \frac{-1}{\omega}\left[\mathrm{Im}\left(\left(\frac{1}{Y_{P_2}} - \frac{1}{j\omega C_{R_1}}\right)^{-1} - \frac{1}{R_{R_1}}\right)\right]^{-1}, \qquad (11)$$

$$R_{R2ex} = \mathrm{Re}\left[\left(\frac{1}{Y_{P_2}} - \frac{1}{j\omega C_{R_1}}\right)^{-1} - \frac{1}{R_{R_1}}\right]^{-1}. \qquad (12)$$

The product $\omega R_{R_2} C_{R_2}$ in equation (10) could be negligible at low frequencies. Thus, to be more precise, the values of C_{R_2} and R_{R_2} are deduced at higher frequencies from the curves of C_{R2ex} and R_{R2ex} where they become constant (Figs 16 and 17).

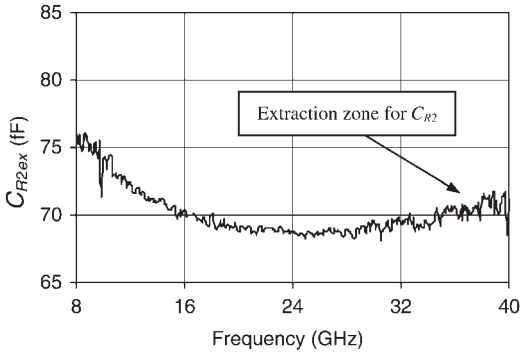

Fig. 16. Variation of C_{R2ex} versus frequency.

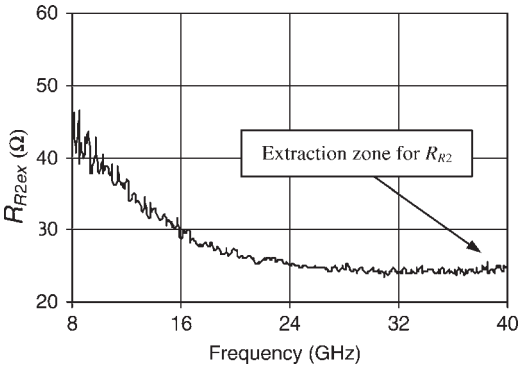

Fig. 17. Variation of R_{R2ex} versus frequency.

Table 2. Extracted values for the elements of the equivalent circuits of the parallel parts of the inductor.

Parameters	Left	Right
C_1 (fF)	140	136
R_1 (Ω)	115	150
C_2 (Ω)	95	71
R_2 (fF)	33	25

The extracted values for the elements of Fig. 15 for both left and right parallel parts of the inductor are summarized in Table 2.

Finally, Figs 18 and 19 compare R_P and C_P extracted from the measurements to their values calculated by using the equivalent circuit in Fig. 15.

C) Results

The complete equivalent scheme of inductors on silicon substrate is the association of series and parallel parts and is given in Fig. 20.

The numerical results are given in Table 3.

A commonly used parameter of a shorted inductor is its quality factor Q defined as

$$Q = -\frac{\mathrm{Im}(Y_{11})}{\mathrm{Re}(Y_{11})}. \qquad (13)$$

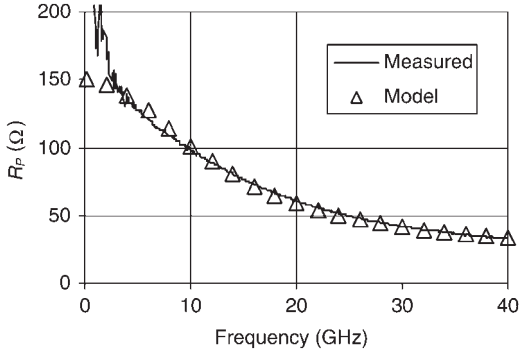

Fig. 18. Comparison of the equivalent series resistance for the right parallel part of the inductor between measurement and equivalent circuit.

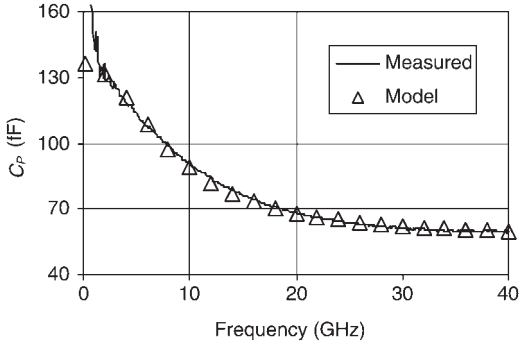

Fig. 19. Comparison of the equivalent series capacitance for the right parallel part of the inductor between measurement and equivalent circuit.

https://doi.org/10.1017/S1759078710000759 Published online by Cambridge University Press

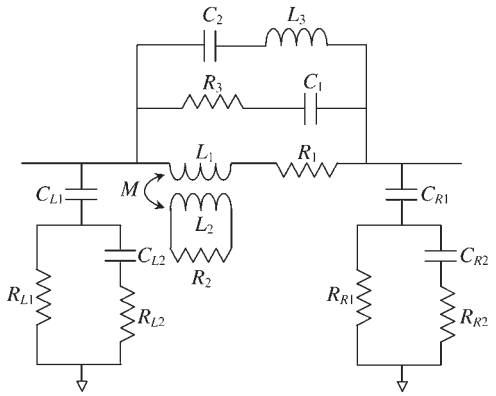

Fig. 20. New model for inductors on lossy substrate.

Table 3. Extracted values for the elements of the equivalent model of the inductor.

$L_1 = 1.24$ nH	$R_3 = -800\ \Omega$	$C_{L1} = 140$ fF	$C_{R1} = 136$ fF
$R_1 = 1.4\ \Omega$	$C_1 = 24$ fF	$C_{L2} = 96$ fF	$C_{R2} = 71$ fF
$k = 0.246$	$L_3 = 2.2$ nH	$R_{L1} = 115\ \Omega$	$R_{R1} = 150\ \Omega$
$\tau = 133$ ps	$C_2 = 4.6$ fF	$R_{L2} = 33\ \Omega$	$R_{R2} = 25\ \Omega$

Figures 21–23 show the comparison between measurement and equivalent circuit in terms of quality factor Q and S-parameters.

We obtain a good agreement between the measurement and the proposed model over the whole frequency band. This result allows applying the proposed model and the extraction procedure of elements to other inductors on lossy substrate.

III. COMPLETE MODEL OF INDUCTOR ON LOSSY SUBSTRATE

A more complete model has been studied in order to explain the negative value for R_3. It is shown in Fig. 24. The results for the element values have been obtained after an optimization. They are summarized in Table 4.

All elements in the complete model of inductance proposed in Fig. 24 have realistic values. This model has thus taken the parasitic coupling effects in the silicon substrate into account. However, the elements cannot be analytically extracted, the model of Fig. 20 is preferred while modeling inductors.

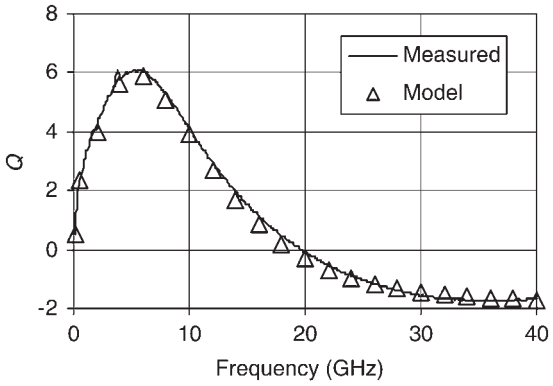

Fig. 21. Comparison of quality factor Q of inductance between measurement and equivalent circuit.

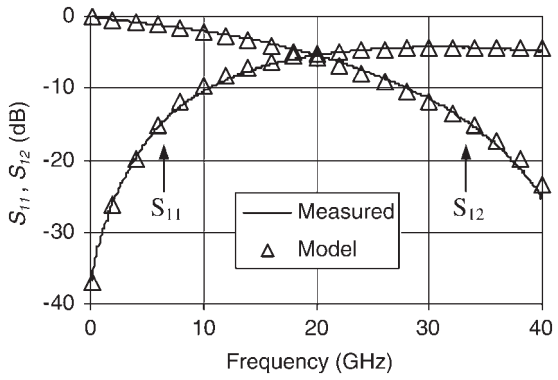

Fig. 22. Magnitude comparison of S_{11} and S_{12} between measurement and equivalent circuit.

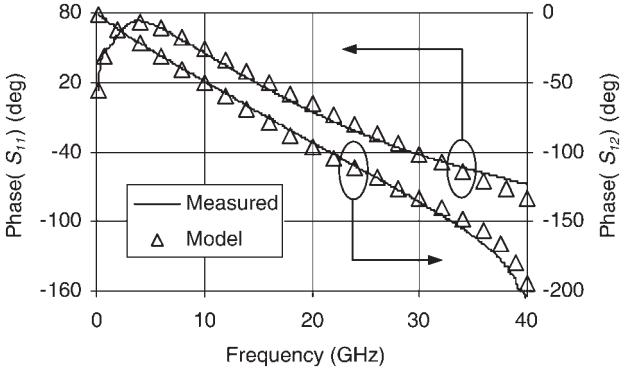

Fig. 23. Phase comparison of S_{11} and S_{12} between measurement and equivalent circuit.

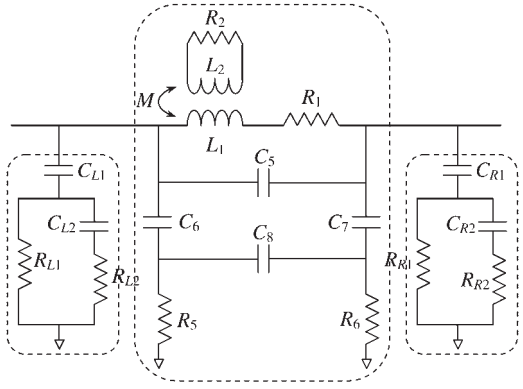

Fig. 24. Complete equivalent scheme taking negative resistance R_3.

IV. APPLICATION TO OTHER INDUCTORS

We have applied the model (Fig. 20) and the extraction procedures of elements presented in Section II to two other inductors

Table 4. Extracted values for the elements of the complete equivalent model of the inductor without negative resistance.

$L_1 = 1.24$ nH	$C_5 = 1$ fF	$R_5 = 270\ \Omega$	$C_{L1} = 105$ fF	$C_{R1} = 95$ fF
$R_1 = 1.4\ \Omega$	$C_6 = 50$ fF	$R_6 = 270\ \Omega$	$C_{L2} = 115$ fF	$C_{R2} = 70$ fF
$k = 0.246$	$C_7 = 50$ fF		$R_{L1} = 330\ \Omega$	$R_{R1} = 380\ \Omega$
$\tau = 133$ ps	$C_8 = 30$ fF		$R_{L2} = 25\ \Omega$	$R_{R2} = 10\ \Omega$

https://doi.org/10.1017/S1759078710000759 Published online by Cambridge University Press

Table 5. Values extracted of elements of the equivalent model of inductor 1.

$L_1 = 1.7$ nH	$R_3 = -750\ \Omega$	$C_{L1} = 170$ fF	$C_{R1} = 180$ fF
$R_1 = 1.5\ \Omega$	$C_3 = 70$ fF	$R_{L1} = 170\ \Omega$	$R_{R1} = 149\ \Omega$
$\tau = 133.3$ ps	$L_4 = 2.1$ nH	$C_{L2} = 110$ fF	$C_{R2} = 78$ fF
$K = 0.2$	$C_4 = 8$ fF	$R_{L2} = 35\ \Omega$	$R_{R2} = 30\ \Omega$

Table 6. Values extracted of elements of the equivalent model of inductor 2.

$L_1 = 2.58$ nH	$R_3 = -1000\ \Omega$	$C_{L1} = 215$ fF	$C_{R1} = 215$ fF
$R_1 = 2.1\ \Omega$	$C_3 = 45$ fF	$R_{L1} = 150\ \Omega$	$R_{R1} = 165\ \Omega$
$\tau = 115.8$ ps	$L_4 = 3.2$ nH	$C_{L2} = 120$ fF	$C_{R2} = 75$ fF
$k = 0.16$	$C_4 = 11.5$ fF	$R_{L2} = 45\ \Omega$	$R_{R2} = 25\ \Omega$

with different geometrical parameters. We have obtained also a good agreement between the measurement results and the equivalent model. Tables 5 and 6 give the results for inductor 1 ($d = 240\ \mu$m, $N = 2$, $W = 20\ \mu$m, $s = 3\ \mu$m) and inductor 2 ($d = 240\ \mu$m, $N = 3$, $W = 20\ \mu$m, $s = 3\ \mu$m).

Figures 25–27 show the variation of the most significant elements of inductances, L_{HF}, R_1, k, against the number of turns N whose diameter d, strip width W, and gap s are, respectively, 200, 20, and 3 μm. The preferred element L_{HF} is the asymptotical value of L_s in region I and corresponds to the nominal value of the inductance. It is determined as

$$L_{HF} = (1 - k)L_1. \tag{14}$$

These results may be interpolated by other on-wafer inductor characterizations and then by efficient electromagnetic simulation results. Thus, by using the extraction procedure that we propose, it will be possible to propose scalable models that are useful for circuit designers.

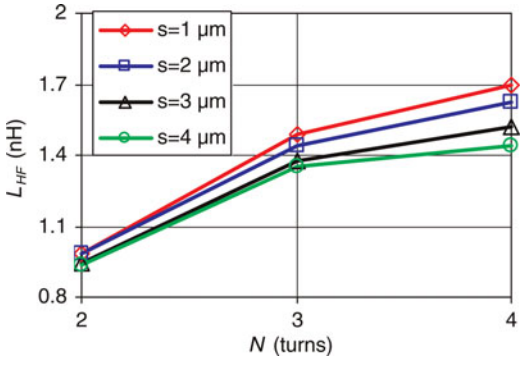

Fig. 25. Variation of L_{HF} versus N for given d, s, and W.

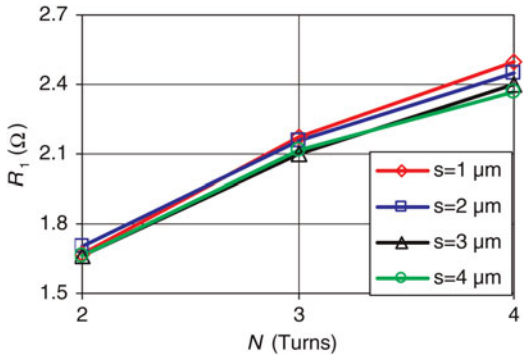

Fig. 26. Variation of R_1 versus N for given d, s, and W.

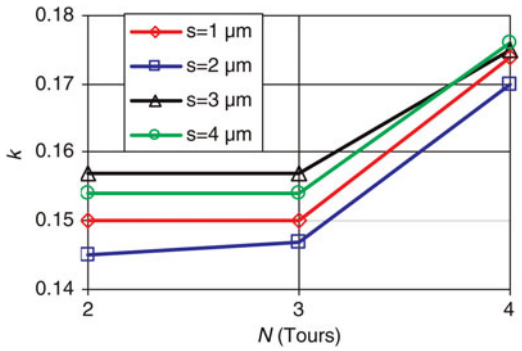

Fig. 27. Variation of R_1 versus N for given d, s, and W.

V. CONCLUSIONS

We have proposed, in Section II, a methodology to extract equivalent circuit of an inductor from 0.1 up to 40 GHz. The eddy currents, the electromagnetic parasitic coupling, and a parasitic resonance have been described in the series part. The different physical effects in the substrate are taken into account in the parallel parts of the model. The different parameters are analytically extracted without the need of an optimization procedure.

The complete model of Fig. 24 contains elements having physical values obtained by optimization procedure. This model allows us to explain the parasitic phenomena in the silicon substrate and the negative resistance R_3 of the model of Fig. 20 where all elements are analytically extracted.

However, our model is sufficient to describe the inductor behavior. Further extraction from electromagnetic simulation will allow our method to propose scale rules for each scheme element.

REFERENCES

[1] Yu Cao, R.A. et al.: Frequency-independent equivalent-circuit model for on-chip spiral inductors. IEEE, J. Solid-State Circuits, **38** (3) (2003), 419–426.

[2] Murphy, O.H.; McCarthy, K.G.; Delabie, C.J.P.; Murphy, A.C.; Murphy, P.J.: Design of multiple-metal stacked inductors incorporating an extended physical model. IEEE Trans. Microw. Theory Tech., **53** (6) (2005), 2063–2072.

[3] Fujishima, M.; Kino, J.: Accurate subcircuit model of an on-chip inductor with a new substrate network, in Proc. Symp. VLSI Circuits, June 17–19, 2004, 376–379.

[4] Ragonese, E.; Biondi, T.; Scuderi, A.; Palmisano, G.: A lumped scalable physics – based model for silicon spiral inductors, in Proc. 10th IEEE Int. Symp. EDMO, November 18–19, 2002, 119–124.

[5] Lee, K.Y.; Mohammadi, S.; Bhattacharya, P.K.; Katehi, L.P.B.: Compact models based on transmission-line concept for integrated capacitors and inductors. IEEE Trans. Microw. Theory Tech., **54** (12) (2006), 4141–4148.

https://doi.org/10.1017/S1759078710000759 Published online by Cambridge University Press

[6] Hasegawa, H.; Furukawa, M.; Yanai, H.: Properties of microstrip line on Si–SiO_2 system. IEEE Trans. Microw. Theory Tech., **19** (11) (1971), 869–881.

[7] Reyes, A.C.; El-Ghazaly, S.M.; Dorn, S.; Dydyk, M.; Schroder, D.K.: Silicon as a microwave substrate, in IEEE MTT-S Int. Microwave Symp. Digest, vol. **3**, 1994, 1759–1762.

[8] Milanovic, V.; Ozgur, M.; DeGroot, D.C.; Jargon, J.A.; Gaitan, M.; Zaghloul, M.E.: Characterization of broadband transmission for coplanar waveguides on CMOS silicon substrate. IEEE Trans. Microw. Theory Tech., **46** (5) (1998), 632–640.

[9] Heinrich, W.: Quasi-TEM description of MMIC coplanar lines including conductor-loss effects. IEEE Trans. Microw. Theory Tech., **41** (1993), 45–52.

[10] Islam, M.S.; Tuncer, E.; Neikirk, D.P.: Accurate quasi-static model for conductor loss in coplanar wave guide, in IEEE MTT-S Int. Microwave Symp. Digest, **1993**, 959–962.

[11] Pfost, M.; Rein, H.-M.; Holzwarth, T.: Modeling substrate effects in the design of high speed Si-bipolar IC's. IEEE J. Solid-State Circuits, **31** (1996), 1493–1501.

[12] Benaissa, K. et al.: RF CMOS on high-resistivity substrate for system-on-chip applications. IEEE Trans. Electron Device Lett., **50** (2003), 567–576.

[13] Chyurm Guo, J.C.; Tan, T.Y.: A broadband and scalable model for on-chip inductors incorporating substrate and conductor loss effects. IEEE Trans. Electron Device, **53** (3) (2006), 413–421.

[14] Williams, D.F.; Marks, R.B.: LRM probe-tip calibrations using non-ideal standards. IEEE Microw. Theory Tech., **43** (1995), 466–469.

[15] Rockwell, S.K.; Bosco, B.A.: On-wafer characterization de-embedding and transmission line optimization on silicon for millimeter-wave applications, in RFIC Symp. Digest Papers, 12–14 June 2005, 561–564.

[16] Ivan, C.H.L.; Minoru, F.: A new on-chip substrate-coupled inductor model implemented with scalable expressions. IEEE, J. Solid-State Circuits, **41** (11) (2006), 2491–2499.

[17] Adam, C.; Watson, D.M.; Pascale, F.; Kyuwoon, H.; Andreas, W.: A comprehensive compact-modeling methodology for spiral inductors in silicon-based RFICS. IEEE Microw. Theory Tech., **52** (3) (2004), 849–857.

[18] Nguyen Tran, L.; Pasquet, D.; Bourdel, E.; Quintanel, S.: CAD-oriented model of a coplanar line on a silicon substrate including eddy current effects and skin effect. IEEE Trans. Microw. Theory Tech., **56** (3) (2008), 663–670.

[19] Patrick Yue, C.; Simon Wong, S.: On-chip spiral inductors with patterned ground shields for Si-based RF IC's. IEEE J. Solid-State Circuits, **33** (5) (1998), 743–752.

[20] Burghartz, J.N.; Rejaei, B.: On the design of RF spiral inductors on silicon. IEEE Trans. Electron Devices, **50** (3) (2003), 718–729.

[21] Horng, T.S.; Wu, J.M.; Yang, L.Q.; Fang, S.T.: A novel modified-T equivalent circuit for modeling LTCC embedded inductors with a large bandwidth. IEEE Trans. Microw. Theory Tech., **51** (12) (2004), 2327–1333.

[22] Chao, C.-J.; Wong, S.-C.; Kao, C.-H.; Chen, M.-J.; Leu, L.-Y.; Chiu, K.-Y.: Characterization and modeling of on-chip spiral inductors for Si RFICs. IEEE Trans. Semiconduct. Manufact., **15** (2002), 19–29.

[23] Long, J.R.; Copeland, M.A.: The modeling, characterization, and design of monolithic inductors for silicon RFICs. IEEE J. Solid-State Circuits, **32** (3) (1997), 357–369.

[24] Tai, C.M.; Liao, C.N.: A physical model of solenoid inductors on silicon substrates. IEEE Trans. Microw. Theory Tech, **55** (12) (2007), 2579–2585.

[25] Ooi, B.L.; Xu, D.X.; Kooi, P.S.; Lin, F.J.: An improved prediction of series resistance in spiral inductor modeling with eddy-current effect. IEEE Trans. Microw. Theory Tech., **50** (9) (2002), 2202–2206.

[26] Kim, S.; Neikirk, D.P.: Compact equivalent circuit model for the skin effect. IEEE Trans. Microw. Theory Tech., **44** (6) (1996), 1815–1818.

[27] Melendy, D.; Francis, P.; Pichler, C.; Hwang, K.; Srinivasan, G.; Weisshaar, A.: A new wideband compact model for spiral inductors in FRICs. IEEE Electron Device Lett., **23** (5) (2005), 273–275.

Linh Nguyen Tran was born in Hai-Duong, Vietnam, on June 15, 1980. He received the M.S. degree in information, system and technology from Ecole Normale Supérieure de Cachan, in 2005. He gained his Ph.D. degree in 2009 at ETIS laboratory.

Emmanuelle Bourdel (M'04) received the Ph.D. degree from Institut National des Sciences Appliquées de Toulouse, France in 1989. She is currently at Ecole Nationale Supérieure de l'Electronique et de ses Applications as an assistant professor. Her current research interests are noise and electrical characterization of monolithic microwave integrated circuits and passive devices and interconnection on chip.

Sébastien Quintanel received the Ph.D. degree in electronics from the University of Limoges, France in 2002. Since 2003 he is an assistant professor at Ecole Nationale Supérieure de l'Electronique et de ses Applications (ENSEA) in Cergy, France and is doing his research at the ETIS laboratory. His research activities concern principally the design and characterization of low noise devices for microwave and millimeter-wave applications.

Daniel Pasquet (M'86, SM'96) is a professor at Ecole Nationale Supérieure de l'Electronique et de ses Applications in Cergy, France and has his research activity at LaMIPS in Caen, France. He gained his Ph.D. at Lille University in 1975. He is currently IEEE France Section chair, MTTS chapter coordinator for Region8, and member of MTT-S "Measurements" Technical Committee (TC-11).

https://doi.org/10.1017/S1759078710000759 Published online by Cambridge University Press